Polymer 222 (2021) 123634

Contents lists available at ScienceDirect

Polymer

journal homepage: http://www.elsevier.com/locate/polymer

Effect of radiant heat exposure on structure and mechanical properties of thermal protective fabrics

Anjani K. Maurya [a,b,c], Sumit Mandal [a,d], Dean E. Wheeldon [a], Jean Schoeller [a,f], Michel Schmid [a], Simon Annaheim [a], Martin Camenzind [a], Giuseppino Fortunato [a], Alex Dommann [b,c], Antonia Neels [b,e], Amin Sadeghpour [a,b,**], René M. Rossi [a,f,*]

[a] Empa, Swiss Federal Laboratories for Materials Science and Technology, Laboratory for Biomimetic Membranes and Textiles, Lerchenfeldstrasse 5, 9014, St. Gallen, Switzerland
[b] Empa, Swiss Federal Laboratories for Materials Science and Technology, Center for X-Ray Analytics, Lerchenfeldstrasse 5, 9014, St. Gallen, Switzerland
[c] ARTORG Center for Biomedical Engineering Research, University of Bern, Murtenstrasse 50, 3008, Bern, Switzerland
[d] Department of Design, Housing and Merchandising, Oklahoma State University, USA
[e] Department of Chemistry, University of Fribourg, Avenue de L'Europe 20, 1700, Fribourg, Switzerland
[f] ETH Zürich, Department of Health Science and Technology, 8092, Zürich, Switzerland

ARTICLE INFO

Keywords:
Thermal protective fibers
SAXS
WAXD
Molecular mechanism
Thermal degradation
Mechanical properties

ABSTRACT

The heat protective performance of thermal protective fabrics is related to the multiscale structure of the fibrous material and the composite design of a multilayered fabric system. In this study, a molecular interpretation is provided to explain the structural changes within fibers to correlate with the mechanical properties of the outermost layer fabric made up of m-aramid blended with (5–10) % p-aramid upon various radiant heat exposures. An increase in crystallinity due to limited polymer chain movement but no change in lamellar spacing was observed when fabrics were exposed below the glass transition temperature which resulted in no change in mechanical properties. A noticeable increase in lamellar spacing and crystallinity was obtained when the temperature during the heat exposures is in the proximity of 375 °C of the fabric layer due to the fibrillar-to-lamellar transformation. Even though no visible changes were observed by scanning electron microscopy (SEM) in the fabric exposed to the aforementioned thermal conditions, we found that their mechanical properties are compromised due to the structural changes within fibers of the fabrics. Therefore, further use of fabrics could be potentially dangerous for the user. Furthermore, for expoheat exposures where the temperature of the fabrics reaches above the degradation point, thermal decomposition occurs which is noticed by its hard and brittle behavior. The inner layers of both the fabric systems mostly remain intact until the thermal degradation of the outermost layers. This study provides an in-depth understanding of molecular mechanisms of structural changes that are in line with changes in the mechanical properties. The understanding of the structure-mechanical property relationship could serve as basic knowledge for the design and fabrication of high-performance fabrics for various fire environments.

1. Introduction

The standards for the performance evaluation of thermal protective clothings were developed after World War II. The National Fire Protection Association is the pioneer in developing the standards for the performance evaluation of thermal protective fabrics used in clothing for firefighters. An improper assessment of the thermal protective performance of the fabric systems could lead to fatalities and injuries to firefighters. The performance of the thermal protective fabric system is usually accessed when it's new. However, the properties of the material might change over time, or exposure to the extreme environments, which is faced by the users, is rarely considered.

* Corresponding author. Empa, Swiss Federal Laboratories for Materials Science and Technology, Laboratory for Biomimetic Membranes and Textiles, Lerchenfeldstrasse 5, 9014, St. Gallen, Switzerland.
** Corresponding author. Empa, Swiss Federal Laboratories for Materials Science and Technology, Center for X-Ray Analytics, Lerchenfeldstrasse 5, 9014, St. Gallen, Switzerland.
E-mail addresses: amin.sadeghpour@gmail.com (A. Sadeghpour), rene.rossi@empa.ch (R.M. Rossi).

https://doi.org/10.1016/j.polymer.2021.123634
Received 23 November 2020; Received in revised form 15 February 2021; Accepted 8 March 2021
Available online 11 March 2021

Some limited efforts over the last few decades have been dedicated to improve firefighter clothing by analyzing thermal aging and proposing the mechanism for the end of life assessment [1–7]. The most commonly used scientific tools for understanding the thermal degradation of the fabrics are thermogravimetric analysis (TGA), differential scanning calorimetry (DSC), and physical appearance which are followed by the determination of the mechanical properties of the fabrics [2–4,7,8]. Rossi et al. have reported that the thermal degradation of the fabrics starts before a visible change of the materials becomes apparent and significantly affects their thermal protective properties [2]. Consequently, the thermal degradation of the fabrics just by the physical appearance might be potentially dangerous for the end-user who will not realize the alteration of the material upon heat exposures [2,8]. Furthermore, Arrieta et al. have studied the thermal degradation of high-performance fibers used in the making of fire protective garments by accelerated thermal aging tests and reported a loss of breaking force retention [3]. They used Fourier-transform infrared (FTIR) analyses to follow the chemical evolution of the materials. Very little evidence of chemical changes in the aged sample was observed and the authors concluded that either aging occurs without significant modification in the chemical structure of the fibers, or FTIR is not an appropriate method to put in evidence such modifications [3]. In a follow-up study, they used X-ray diffraction, Raman spectroscopy, and DSC to investigate the thermal aging effect on the crystallinity of Kevlar®-PBI blended fabrics and reported a gradual increase in the crystallinity with temperature and aging time [5]. Most recently, Schmid et al. attempted to study thermal degradation by developing a theoretical model, which analyses the critical heat transfer through the fabric system, based on its thermal resistance [9]. They reported that synthetic polyester underwear worn underneath heat-protective clothing can withstand without any damage of a 4s flame engulfment exposure with an adequate thermal resistance of the outer layer [9].

The commercially available firefighter thermal protective fabrics are consisting of multi-layered fabric systems [10]. A common material used for the outermost layer (i.e. outer shell fabric) for thermal protective fabrics is poly (meta-phenylene isophthalamide) (m-aramid) blended with (5–10) % of poly (para-phenylene isophthalamide) (p-aramid). The m-aramid fibers have excellent heat and flame resistance, high chemical resistance, and self-extinguishing flame retardant properties [11]. Blending with (5–10)% of p-aramid fibers provides a higher structural rigidity to the fabric due to the extreme structural order of the polymer chains in the p-aramid fibers [11]. The moisture barrier in the middle or second layer designed to prevent the fire hose water passing through the clothing system to prevent the wearer from being soaked. The thermal liner as the third/innermost layer is responsible for heat transfer management.

As thermal protective fabrics consist of polymeric fibers, they exhibit structure in a multiscale domain (micro-nm-Å scale) which critically influences their mechanical properties [12,13]. Therefore, a multiscale analytical approach involving electron microscopy (EM), small-angle X-ray scattering (SAXS), and wide-angle X-ray diffraction (WAXD) is required to decode the structural changes upon heat exposures to correlate it with the change in its mechanical properties. In the past, efforts have been made to understand structural changes within the fibers using EM, SAXS, and WAXD due to mechanical deformation and annealing [12,14–18]. Ran et al. have described the changes in the structure during the deformation of Kevlar fibers by simultaneous SAXS and WAXD techniques using synchrotrons [12]. They observed transitions between crystalline, amorphous, and mesomorphic fractions during the deformation of Kevlar® 49 fibers that originally consists of 50% crystalline, 30% amorphous, and 20% of the fraction (mass) mesophase. Murthy et al. have investigated the annealing and deformation effect on the structural changes into the Nylon 6 fibers [15,16,18]. They reported that secondary crystallization during annealing occurs at the expense of the oriented amorphous fraction of the fibers. However, a complete understanding of the molecular mechanism underlying structural changes within thermal protective fabrics and the correlation with the mechanical properties upon radiant heat exposures is still missing.

In this study, we investigated the multiscale structural changes in thermal protective fabrics upon various radiant heat exposures and correlate it with changes in their mechanical properties. In general, aramid fibers based fabric are used for thermal protective clothing in Europe and all over the world. Therefore, we considered commercially available multi-layered aramid fabrics systems with the outer shell, moisture barrier, and/or thermal liner in this study. The structural changes within fibers were investigated at μm-nm-Å scale by combining different characterization techniques such as SEM, TGA, DSC, SAXS, WAXD, and mechanical properties were accessed by performing tensile tests on the fabrics exposed to various thermal conditions.

2. Materials and methods

2.1. Fabric selection

Two commercially available multilayered high-performance fabric systems (namely TG1 and TG2) were selected for this study. The selected fabric systems are commonly used for thermal protective clothing worn by firefighters. TG1 and TG2 were consists of two and three layers, respectively. The layer-by-layer fiber materials and their physical properties are provided in Table 1 and their images are shown in supporting figure S1.

2.2. Heat exposure experiment

Standardized equipment according to ISO 6942 was used for heat exposure. The setup consisted of an electrically heated radiant source (six silicon carbide heating rods) and a calorimeter positioned on a sliding frame on which the samples were fixed. The heat flux was adjusted by changing the distance of the calorimeter to the radiant source. Fabric systems were exposed to various thermal conditions as listed in Table 2. The average temperature at each layer of the fabric systems was measured by placing the temperature sensors in the front and in between the layers. A schematic presentation of the positions of the sensors along with the image of the radiant heat setup is shown in supporting figure S2. Based on the literature, it has been found that firefighters mainly expose to low to medium range radiant heat [19]. As per the ISO 6942 standard, mainly low to medium radiant heat lies in between 10 and 40 kW/m^2. Therefore, we selected this heat flux range for this study. Also, firefighters need to work in the radiant heat exposure for a longer duration depending upon the firefighting situation. Therefore, two different times set were chosen within 1 min for the comparative analysis.

Four thermal conditions (I − IV) were set based on the heat flux and the exposure time, i.e. I = 0, II = 10, III = 20, IV = 30 and 40 kW/m^2, with 30 and 60s exposure time for each heat flux, except 40 kW/m^2 flux, for which sample was exposed only for 30s. The thermal condition I corresponds to the non-heated (NH) samples. NH samples were used for comparing the relative changes in the structure and mechanical properties upon heat exposures. Thermal condition II corresponds to the temperatures below the glass transition temperature (T_g) of m-aramid fibers (Fig. 2). Thermal condition III was chosen where the average temperature was above T_g and below the T_x = 375 °C for m-aramid fibers. Here, T_x is the temperature reported in the literature about which m-aramid starts to slowly melt and/or decompose [20–23]. However, no clear evidence of melting point (T_m) is reported in the literature for m-aramid fibers [22,23]. Therefore, we call this temperature as T_x in this study. Finally, thermal condition IV was chosen above the degradation temperature (T_d) of m-aramid fibers to investigate the thermal degradation of the fabrics.

Table 1
The fiber materials and physical properties of the selected fabric system.

Fabric Systems		Layer Name	Materials	Physical Properties				
				Weight (g/m^2)	Thickness (mm)	Air Permeability ($cm^3/cm^2/s$)	Thermal Resistance (K. $m^2/W.10^{-3}$)	Evaporative Resistance (Pa. m^2/W)
Turnout Gear (Outer layer to inner layer; outer layer facing the source)	TG1	TG1-1	m-aramid blended (5–10) % p-aramid (Plain Ripstop (23 warp/cm X 21 weft/cm))	258	0.5	0	80.0	15.8
		TG1-2	3-layers GORE-TEX Airlock (InnL) Polytetrafluorethylene (PTFE) dots on nonwoven (spunlaced m.aramid) fabric side of a GORE-TEX membrane laminated with an m-aramid fabric	345	1.5			
	TG2	TG2-1	m-aramid blended with (5–10)% p-aramid (Plain (40 warp/cm X 35 weft/cm))	175	0.38	0	71.0	16.8
		TG2-2	(PTFE coated on needle punched nonwoven web of 25% m-aramid/25% p-aramid/50% Basofil)	90	0.38			
		TG2-3G + TG2-3Y	Nonwoven m-aramid + quilted with 50% m-aramid/50 FR Viscose fabric	158	0.59			

Table 2
The selected fabric systems and corresponding radiant heat exposure conditions.

Fabric systems	Thermal conditions	Heat flux - Exposure time (kW/m^2) - (seconds)
TG1 & TG2	I	Non-heated (NH)
	II	10–30
		10–60
	III	20–30
		20–60
	IV	30–30
		30–60
		40–30

2.3. Scanning electron microscopy (SEM)

The outermost layer of the fabric systems exposed in thermal conditions I – IV were imaged with SEM (Hitachi S-4800, Hitachi-High Technologies, Illinois, USA) with an acceleration voltage of 2 kV and a current of 10 μA. Before SEM imaging, all samples were sputter-coated with a conducting layer of gold-palladium with a thickness of 8 nm. SEM was used to access the microscale surface morphology of the fabrics upon heat exposures.

2.4. Thermogravimetric analysis (TGA) and differential scanning calorimetry (DSC)

TGA measurements were performed on a NETZCH TG209 F1 Iris instrument (NETZSCH, Germany) to study the thermal degradation of the fabrics. Specimens of around 5 mg were cut from the different layers of the fabric and heated from 110 to 800 °C at a heating rate of 10 °C/min. The measurement was performed using a mixture of 80% O_2 and 20% N_2 to study the impact of oxygen during the heating.

DSC curves were recorded on a NETZCH DSC 214 Polyma (NETZSCH, Germany) under the aforementioned gas mixture at a heating rate of 10 °C/min to measure the typical transitions (glass transition, melting temperature, or recrystallization temperature). The specimens of 5–7 mg were compressed to the bottom of an aluminum crucible with a pierced lid and heated from 50 °C to 300 °C. The data was analyzed using the associated software (NETZCH Proteus Thermal Analysis Version 7.1.0).

2.5. Small angle X-ray scattering (SAXS) and wide angle X-ray diffraction (WAXD)

SAXS and WAXD are powerful techniques to characterize the nm-Å scale structural features in the materials [24,25]. SAXS and WAXD experiments were performed on a Bruker Nanostar instrument (Bruker AXS GmbH, Karlsruhe, Germany). The instrument was equipped with a pinhole collimation system and a micro-focused X-ray Cu source (wavelength of Cu Kα = 1.5406 Å) providing a beam with a diameter of about 400 μm and a 2D MikroGap™ technology-based detector (VÅNTEC-2000) with 2048 × 2048 pixels with a pixel size of 68 × 68 μm^2. The instrument was equipped with a semi-transparent, custom-built beamstop. The X-ray beam impinged the fabric samples in transmission mode. The scattering frames were recorded at room temperature in moderate vacuum conditions of about 10^{-2} mbar pressure to reduce air scattering. Before the experiments, the sample-to-detector distances (SDD) were calibrated with a standard silver behenate powder for SAXS (SDD 107 cm) and a standard corundum sample for WAXD (SDD 5 cm). 1D-radial and azimuthal profiles were extracted using the DIFFRAC.EVA (Bruker AXS, version 4.1).

A bundle of extracted fibers (wherever possible) or pieces (about 5 × 5 mm^2) of the fabrics were used for measuring the SAXS and WAXD frames for 30–45 min. Three SAXS and WAXD frames were recorded for each sample. The background frames were recorded for equal amount of exposure time without any sample in the X-ray beam. After normalizing the 1D extracted scattering profiles by the transmitted intensity, the background was subtracted from the corresponding scattering profile of the sample to remove the contribution of residual air scattering.

2.6. Porod-correlation peak model fitting of SAXS data

To quantify the nanostructure information, often fitting of the 1D-radial profiles is required by using a suitable model. SAXS profiles obtained from the fiber samples can be described by the Porod-correlation peak model given by equation (1). The details of this model are described elsewhere [13].

$$I(q) = \frac{A}{q^{\alpha}} + \frac{B}{1 + \left(\frac{2\,|q-q_0|}{w}\right)^{m}} \quad (1)$$

where A and B are multiplying factors; α denotes the Porod exponent, q_0 are the peak position and w shows the full width half maximum (FWHM) of the peak and m is a fitting parameter for correction of the peak shape (when $m = 2$ a Lorentzian peak function is assumed).

The average spacing between repeating amorphous and crystalline domains (i.e. lamellar spacing) is calculated from the peak position by using equation (2).

$$d = \frac{2\pi}{q_o} \tag{2}$$

All the fittings were performed in MATLAB (R2019b).

2.7. Determination of crystallinity by rietveld fitting of WAXD data

To determine the degree of crystallinity in the radiant heat exposed fabric samples, Rietveld fittings and related calculations were performed on WAXD data using the TOPAS software [26]. Rietveld fitting is based on the least-square method to minimize the difference between the model-based calculated and experimentally obtained diffraction patterns [27,28]. Preferred orientation was included in the fitting since the experiments were performed on bundles of fibers orientated in the crystallographic c-axis. The instrumental broadening and peak shape were extracted from a measurement of the standard corundum calibration sample. The crystalline phase information was obtained from the database (m-aramid and p-aramid with Cambridge crystallographic data center (CCDC) no. 1207433 and 1176049, respectively). The m- and p-aramid phases were fitted together with the amorphous part which was included as a broad hump in the diffraction profile after background correction. As a result, the degree of crystallinity was obtained.

2.8. Mechanical strength experiment

Mechanical properties were assessed using tensile tests (ZwickRoell GmbH) according to EN29073-3. Ten dog bone-shaped samples of 75 mm length (gauge length 50 mm) and 4 mm width were extracted from each layer and prepared for tensile testing. An image of the specimen is shown in supporting figure S7. The testing speed was set to 10 mm/min with a pretension of 0.5 cN. Depending on the condition of the sample a calibrated 10 N or 100 N gauge was used to assess tensile force. The measured force-elongation curves were used for calculating the engineering stress-strain curve as the input for the determination of Young's modulus, tensile strength, and maximum elongation at the break of each layer of fabric systems. The specimens were conditioned at room temperature (21 °C) and relative humidity of about 65% according to ISO 139.

2.9. Calculation of Young's modulus of the of fabrics

The Young's modulus (E) represents the resistance of the materials from non-permanent deformation when a tensile force is applied to it. Young's modulus is calculated from the slope of the stress vs strain curve in the elastic deformation region given by equation (3).

$$E = \frac{\sigma}{\varepsilon} \tag{3}$$

Here, σ is the applied stress (Pa or $kg{\cdot}m^{-1}{\cdot}s^{-2}$) and ε is the strain, which is unitless.

$\sigma = \frac{F}{A}$; $\varepsilon = \frac{\Delta L}{L_o}$;F is the applied force (N), A is the cross-sectional area (m^2) of the material, ΔL is the elongation (m) and L_o is the gauge length (m). Therefore, we obtain

$$E = \frac{F}{A}\,\frac{L_o}{\Delta L} \tag{4}$$

In this study, the force per unit elongation was obtained from the slope of the force-elongation curve measured for each layer of the fabric systems at low elongation. The cross-section area was calculated from the thickness and width of the fabric samples. The thickness of the original fabrics was measured using ISO 5084 standard under 1 kPa compression.

3. Results and discussion

3.1. The outermost layer of the fabric systems

3.1.1. Thermal analysis of the fabrics (TGA and DSC)

The outer layers of the two fabric systems were first evaluated with respect to thermal properties, both by looking at starting degradation temperatures (TGA) as well as internal thermal transitions (DSC). The TGA and DSC plots of TG1-1 and TG2-1 are shown in Fig. 1 (a) and (b), respectively. TGA experiments were performed to obtain the degradation point of materials. The degradation point is obtained by determining the first-order derivative of the TGA mass change curve over temperature.

As seen in the TGA curves, after an initial loss of bound water (moisture) around 100 °C (3 wt%), both samples exhibited a similar starting decomposition temperature where the weight loss started around 400 °C [22]. The transition around 432 °C is attributed to the starting thermal degradation point (T_d) of the m-aramid fabrics. Finally, the second inflection at 557 °C was attributed to the starting degradation of the p-aramid contained in the fabric [8].

Unfortunately, due to the low interchain fractional free volume of aramids, no conclusive information about the typical transitions of the fabrics could be obtained from DSC measurement. The first endothermal transition is attributed to the loss of bound water. Furthermore, the glass transition temperature was not clearly defined on the DSC curves. Therefore, we fixed the glass transition temperature at about 260 °C according to values given in the literature for m-aramid fibers [29–31]. The endothermic peak in the curve shown at 253 °C might be due to the melting of the static dissipative fiber.

3.1.2. The distinction between thermal conditions (I-IV) with respect to the temperature

The temperature course for each layer was measured for thermal conditions I-IV. The temperature course in time from each sensor are plotted for all thermal conditions in the supporting figure S3 and S4 for TG1 and TG2 fabric systems, respectively. The average temperature of the outermost layer of both fabric systems was extracted by taking the mean of temperature sensors placed in the front and backside of the same layer. Average temperatures measured at different heat exposures are shown in Fig. 2. It is interesting to note that the measured temperature value of the inner sensor for the TG1-1 layer differs from the outermost sensor of the same layer which is also indicated by high error bars in Fig. 2. The reason for such difference could be due to expanded PTFE dots in the TG1-2 layer which provided more air gap and hinder the placement of the sensors for the TG1 fabric system. However, TG2 is consisting of fabrics without expended PTFE dots which provide better placement of the sensors in front as well in the back of the fabric layer which contributes less error in the temperature measurement.

In Fig. 2, It can be observed that the samples exposed in thermal condition II are below T_g, under thermal condition III are in the proximity of T_x, and under thermal condition IV are approaching or above the T_d of m-aramid fibers. The average temperature of the first layers in both fabrics correlates well with the values obtained from our TGA, DSC measurement and the literatures [8,22]. The first plateau and change of steepness can be explained by the endothermal nature of the glass transition resulting in a less steep evolution of the average temperature as well as a plateau before the transition. The same behavior was observed when reaching values close to the T_x which also corresponds to an endothermic transition where the enthalpy of the fabrics increases. No significant changes in the average temperature within the fabrics could be observed when reaching the degradation temperature.

3.1.3. Surface morphology as accessed from SEM

Each layer in both fabric systems was investigated after their respective heat exposures. It was detected directly from the physical appearance that the outermost layer of both fabrics was more affected

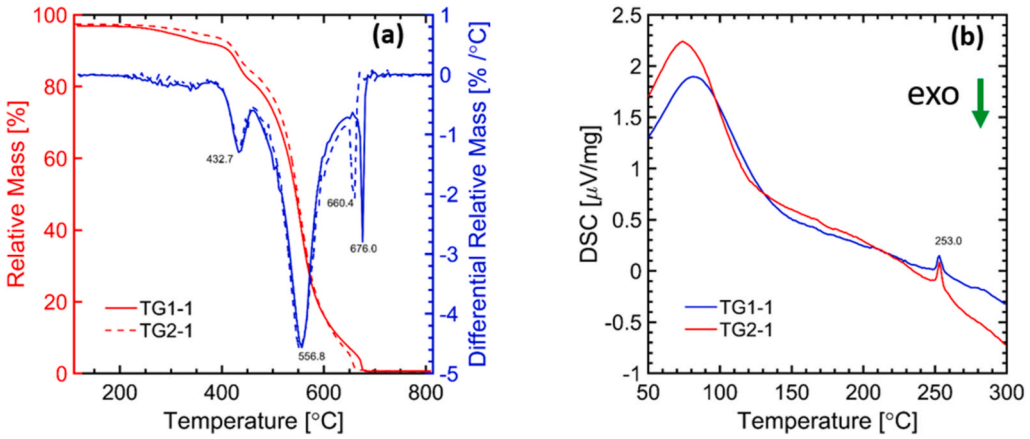

Fig. 1. (a) TGA curves TG1-1 and TG2-1 and their corresponding first order derivation of the relative mass change over temperature. (b) DSC curves of TG1-1 and TG2-1 fabrics.

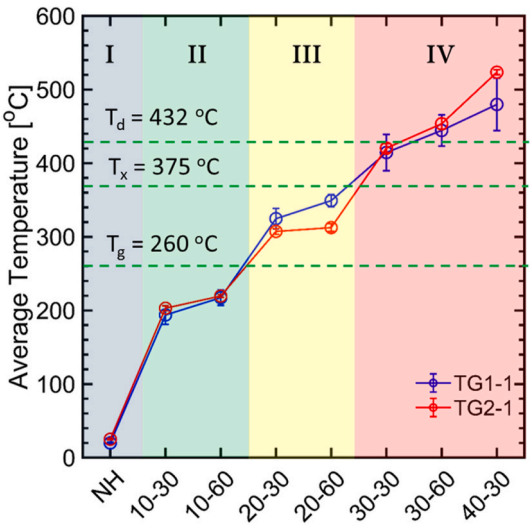

Fig. 2. Average measured temperature of the outermost layer for both fabric systems plotted over four thermal conditions I-IV. Quantitatively, i.e. I = 0, II = 10, III = 20, IV = 30 and 40 kW/m^2, for 30 & 60s exposures for each heat flux except 40 kW/m^2 flux for which sample was exposed only for 30s. The X-axis represents the samples with the flux and their corresponding exposure time and color schemes are indicating the thermal conditions I-IV. Green dashed lines are representing the T_g, T_x and T_d of m-aramid. (For interpretation of the references to color in this figure legend, the reader is referred to the Web version of this article.)

due to the radiant heat exposures. SEM micrographs of the outermost layers in both fabrics are shown in Fig. 3 for thermal conditions I-IV. In both fabrics, no microscopic surface changes were noticed for thermal conditions I-III. The thermal degradation of the fibers is visible in the samples exposed under thermal condition IV as the temperature in this thermal condition was either approaching or above the T_d of the m-aramid (Fig. 2). The increase in degradation could be directly noticed in the SEM images of fabric in thermal condition IV on increasing the flux from 30kW/m2 to 40kW/m2 which leads to higher mass loss evident in TGA.

3.1.4. Understanding structural changes in the nm-Å scale by SAXS and WAXD

SAXS and WAXD experiments were performed on bundles of fibers extracted from the fabrics for thermal conditions I-III and a small piece of the fabric sample for thermal condition IV, as the extraction of fibers was not possible. SAXS and WAXD studies were of particular interest for fabrics exposed to thermal conditions I-III as no visible changes were observed with SEM compared to the NH sample. 2D-SAXS profiles of the samples exposed at thermal conditions I-III are shown in Fig. 4. 2D-SAXS represents a characteristic scattering profile of fiber consisting of a streak signal lateral to alignment and correlation peak along the fiber alignment direction. The streak is representative of the fibrillar structure within fibers [12,13,15,32]. A reduction in streak intensity could be observed in 2D-SAXS profiles for the samples exposed under thermal conditions III compared to the samples under thermal conditions I and II. The decrease in streak intensity was quantified by extracting azimuthal profiles (lateral to the fiber alignment in 0.5–1 nm^{-1} q-range; supporting figure S5) for thermal condition III samples compared to the thermal condition I and II. A decrease in azimuthal streak intensity (or area under the peak) was observed for the samples under thermal conditions III, which indicates the drop in fibrillar structure inside the fiber treated under this thermal condition.

Furthermore, the 1D radial profiles in the fiber alignment direction were extracted by performing a 30° wedge azimuthal integration as indicated in Fig. 4. The extracted 1D radial profile after background subtraction is shown in Fig. 5 (a) and (b) for TG1-1 and TG2-1, respectively. The 1D extracted radial profiles for TG1-1 and TG2-1 show an exponential decay that could be explained by the Porod law and the correlation peak for the samples exposed in thermal conditions I-III. Therefore, a Porod-correlation peak model was used to fit each profile given by equation (1). A Porod exponent of 4 indicates the 3-dimensional smooth interface of the scatterers while a Porod exponent between 3 and 4, indicates a rather rough interface [33]. A Porod exponent of about 3.5 was obtained for TG1-1 and TG2-1, which indicates the relatively rough interface of the scatterers.

The origin of the correlation peak in the fiber is described by the repetition of amorphous and crystalline (i.e. lamella) domains which constitute the fibrillar structure [13,16,17]. The peak position corresponds to the average distance between the two lamellae, also known as lamellar spacing. The lamellar spacing was determined by equation (2) and plotted in Fig. 6 for TG1-1 and TG2-1. A lamellar spacing of 9.9 ± 0.2 nm and 10.0 ± 0.1 nm was obtained for the NH samples (i.e. thermal condition I) of TG1-1 and TG2-1, respectively.

For samples exposed in the thermal condition II, no significant change in the lamellar spacing was observed compared to the NH samples. The reason for no change in the lamellar spacing is probably due to the limited supplied energy to the fabric which is not enough to produce changes in the nanostructure within the fibers.

A noticeable increase in the lamellar spacing (Fig. 6) along with an increase in correlation peak intensity (Fig. 5 (a) & (b)) was observed for the samples exposed in thermal condition III compared to the NH sample. Several molecular interpretations such as refolding by solid-state

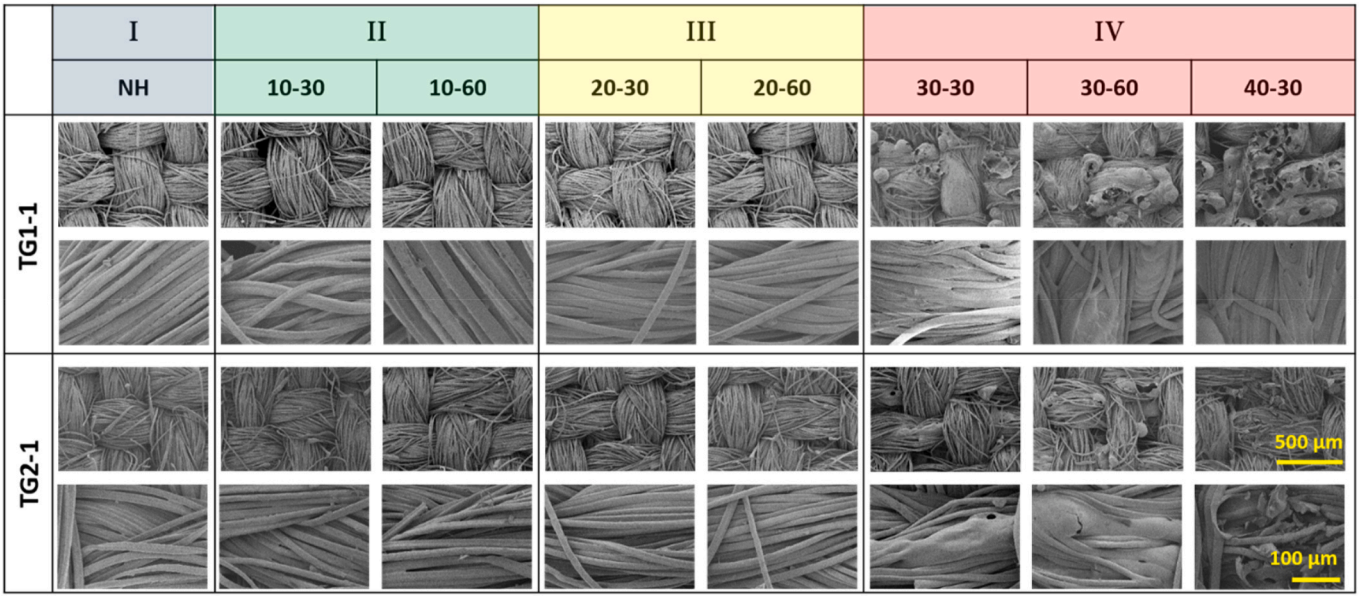

Fig. 3. SEM micrographs of the outermost layer (TG1-1 and TG2-1) of both fabric systems exposed to thermal conditions I-IV.

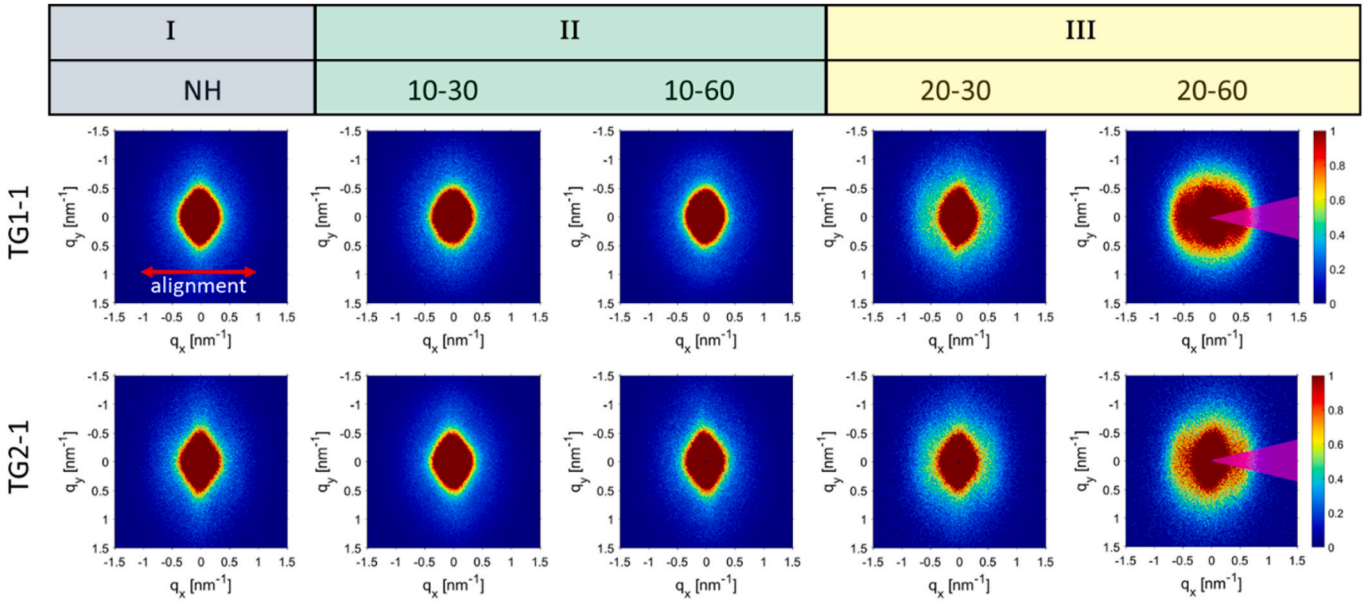

Fig. 4. Normalized (by transmission intensity at beam center) 2D-SAXS profiles of the first layer of the fibers exposed to the thermal conditions I – III.

diffusion, the selective melting of the thinner lamellae and recrystallization to thicker lamellae, and the fold surface pre-melting have been reported to explain the increase in the lamellar spacing in semi-crystalline polymeric materials due to the annealing effect [14,17,34,35]. It is reported that when most of the polymeric fibers are annealed at sufficiently high temperatures (near the melting point of the polymeric material), a transformation from a fibrillar to a lamellar morphology takes place [17,36,37]. In our study, when the temperature of the fabrics exposed in the thermal condition III was sufficiently high and near to the T_x of the m-aramid fibers, the additional molecular mobility allows the lateral alignment of lamella within the neighboring microfibril as well as the growth of lamellar thickness through a solid-state refolding process [17]. This process goes along with a rearrangement of the amorphous chain segments leading to fibrillar-to-lamellar transformations [34,36,37]. The fibrillar-to-lamellar transformation is also supported by a drop in the streak signal which corresponds to the fibrillar structure. Therefore, the merging of nearby lamella with amorphous demains which leads to fibrillar-to-lamellar transformations could be the reason for the increase in the average spacing between the newly transformed lamella in the samples exposed in thermal condition III.

The correlation peak in the SAXS profiles disappeared for the samples exposed in thermal condition IV as shown in Fig. 5 (a) and (b). The corresponding temperature for the samples exposed under thermal condition IV is either approaching or above the T_d (Fig. 2) of the m-aramid fibers. It means that the material undergoes a molecular structure breakdown due to thermal degradation. Therefore, the correlation peak is disappeared.

WAXD experiments were performed to analyze the changes in the molecular structure of the polymer fibers upon heat exposures. The 2D-WAXD profiles of TG1-1 and TG2-1 are given in the supporting figure S6 for thermal condition I-III. The 1D extracted radial profiles are shown in Fig. 7 (a) and (b) for TG1-1 and TG2-1 for all four thermal conditions.

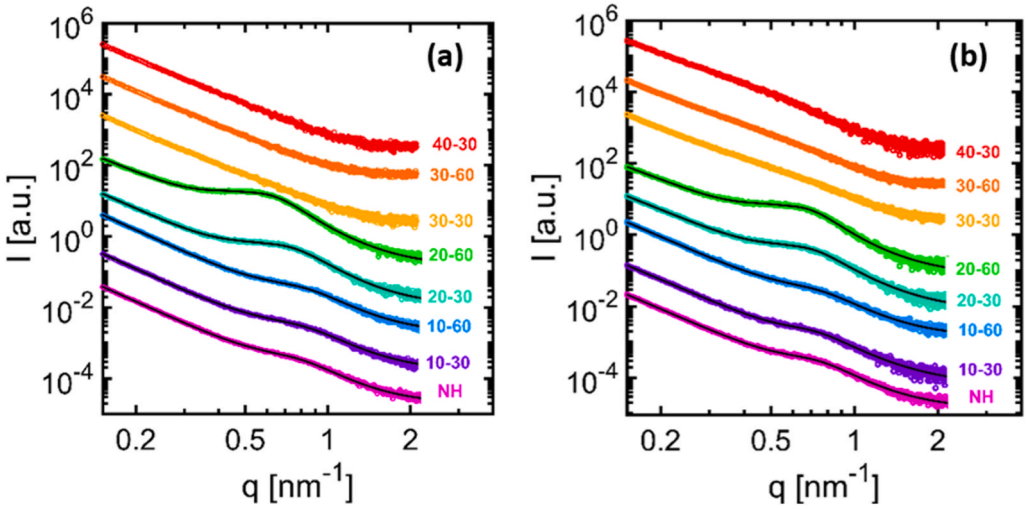

Fig. 5. 1D extracted radial profiles in fiber direction by performing a 30° wedge azimuthal integration for the thermal conditions I-IV for (a) TG1-1 and (b) TG2-1. The continuous black line represents the fitted curve with the Porod-correlation peak model for thermal conditions I-III.

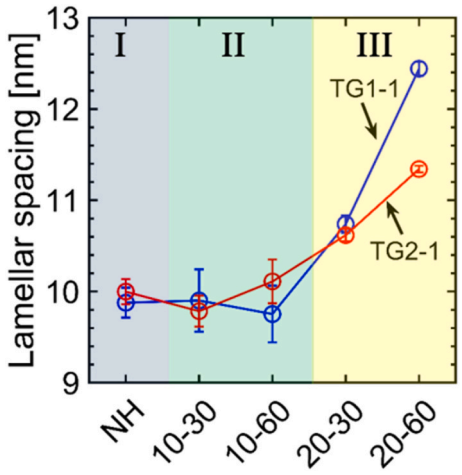

Fig. 6. The average lamellar spacing for TG1-1 and TG2-1 for thermal conditions I-III.

The crystal structure of m-aramid is triclinic with unit cell parameters of a = 5.27 Å, b = 5.25 Å, c (fiber axis) = 11.3 Å, α = 111.5°, β = 111.4° and γ = 88.0° with the crystallographic space group P1 [38]. On the other hand, p-aramid is monoclinic (pseudo-orthorhombic) with unit cell parameters of a = 7.87 Å, b = 5.18 Å, c (fiber axis) = 12.9 Å and α = β = γ = 90°, and possesses Pn or $P2_1/n$ space-group symmetry [39]. The molecular packings with the unit cell of the m-aramid and p-aramid fibers are shown in Fig. 7 (c). Simulated diffraction patterns with a FWHM of 0.1° based on the above mentioned unit cells and symmetries for m- and p-aramid are shown at the bottom in Fig. 7 (a) and (b) for TG1-1 and TG2-1, respectively.

The total percentage of crystallinity (including m- and p-aramid phases) for TG1-1 and TG2-1 was obtained from the Rietveld fitting which is plotted in Fig. 8. All diffraction profiles show broad peaks on a shallow amorphous hump. The crystallinity was estimated for the NH samples with 28% and 26% for TG1-1 and TG2-1, respectively. An increase in crystallinity was obtained in thermal conditions II and III compared to the NH samples. This is in line with Arrieta et al. who also reported a gradual increase in crystallinity with temperature and aging time for the Kevlar®-PBI blend fabrics [5].

For the samples exposed in thermal condition II, a relative increase in crystallinity was observed for TG1-1 and TG2-1 fabrics which is due to the limited movement of polymer chains, leading to a higher crystalline perfection [16,40]. Similar to SAXS, major changes in the WAXD profiles were observed in the sample exposed to the thermal condition III. An increase in the intensity of the (100), (101) & (011), and (110) reflections could be noticed directly in Fig. 7 (a) and (b), resulting in an increase in the crystallinity for both fabrics (Fig. 8). Such an increase in crystallinity is explained by the merging of lamella domains through the amorphous polymer chain rearrangement due to sufficient energy which leads to the fibrillar-to-lamellar transformation.

For the samples exposed to thermal condition IV, high-intensity peaks corresponding to the m-aramid disappeared and only a broad hump was observed in the diffraction profile together with two peaks ($1\bar{1}0$) and (200) belonging to p-aramid. This is the signature of a breakdown of the molecular structure of the m-aramid fibers due to the thermal degradation of the samples. The high-intensity reflections from the fibers corresponding to p-aramid were still observed in the thermal condition IV samples beacuse the applied temperature was above the degradation temperature of the m-aramid but still below the degradation point (557 °C) of the p-aramid fibers fi. A schematic presentation of the above molecular interpretation in structural changes within fibers for the thermal conditions I – IV has been summarized in Fig. 9.

3.1.5. Correlation between structural and mechanical properties of fabrics upon heat exposures

The mechanical properties of the fabric materials are related to the organization of polymer chains within the fibers and the macro textile structure [41,42]. Therefore, it is important to investigate the mechanical properties of the fabrics related to various heat conditions to understand the correlations with structural changes observed by SAXS, WAXD, and SEM. This is needed to access the further usage of the fabric systems upon heat exposures. 10 samples were analyzed for each thermal condition and the corresponding force-elongation curves are shown in the supporting figure S8 and S9 for TG1-1 and TG2-1, respectively.

The force-elongation curve of fabrics usually demonstrates an initial low slope due to decrimping and crimp-interchange [43–45]. Thereafter, fibers in the fabrics begin to extend upon increasing the force and demonstrate elastic and plastic domains. Therefore, the mechanical properties of the fabrics depend on the mechanical properties of the polymeric fibers and the macro-structure of the fabrics [43]. As the macro-structure of the outermost layers remains the same in our study, thus fabric mechanical property would mainly depend on their structural modification within fibers upon various heat exposures. Various methods for analyzing the mechanical behavior of the semi-crystalline

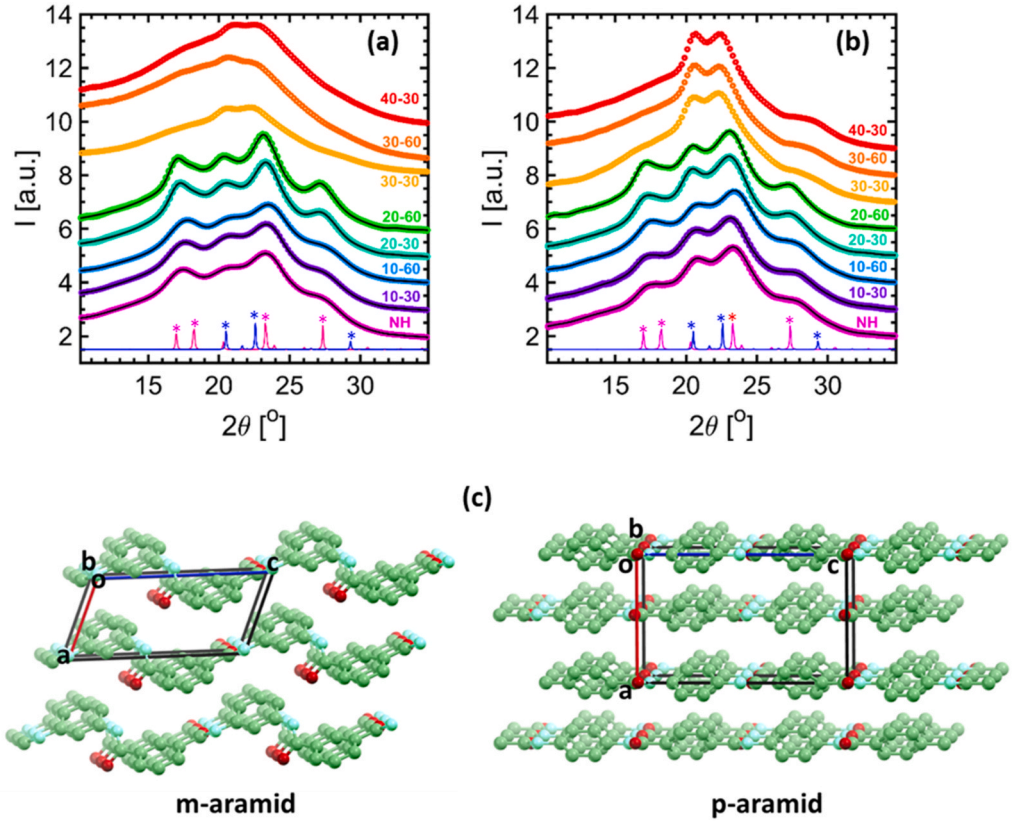

Fig. 7. 1D extracted radial profiles from 2D-WAXD for thermal conditions I-IV for (a) TG1-1 and (b) TG2-1 fabric layer. The continuous black line represents the fitted profile in TOPAS. Simulated diffraction patterns of m-aramid (*, blue) and p-aramid (*, pink) are shown at the bottom of each plot. The pink star symbols represent high-intensity diffraction peaks originating from (10$\bar{1}$) & (01$\bar{1}$), (100) & (010), (101) & (011), and (110) planes of m-aramid and the blue star symbols represent the (1–10), (200) and (211) planes of p-aramid from left to right direction. 2θ is given with respect to Cu Kα radiation (λ = 1.5406 Å). (c) Molecular packing with unit cells of m-aramid (*Cambridge crystallographic data center* (CCDC) no. 1207433) [38] and p-aramid (CCDC no. 1176049) [39]. (For interpretation of the references to color in this figure legend, the reader is referred to the Web version of this article.)

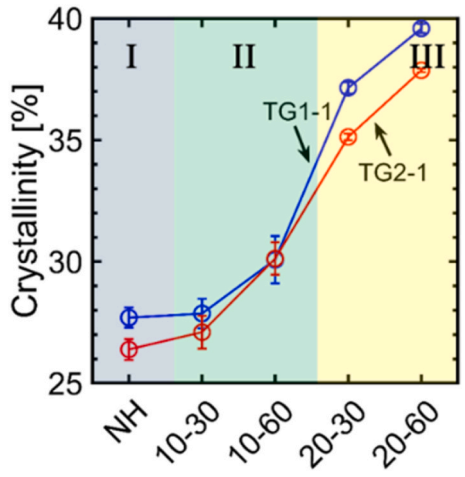

Fig. 8. Crystallinity determined from WAXD data analysis for thermal conditions I-III for TG1-1 and TG2-1.

polymeric materials have been reported in the literature [41,42,46]. The theory of rubber elasticity has been the starting point of the explanations and then later on modifications due to the presence of crystalline domains are considered as (a) rigid fillers, (b) connectors between chains, and (c) regions of greater stability which grow at the expense of the pulling chains in the amorphous regions into extended forms [42,46].

The initial low slope in the force-elongation curve due to the straightening of the crimp fibers is observed for the sample exposed in the thermal condition I and II of TG1-1 and TG2-1 (supporting figure S8 and S9). Subsequently, the force-elongation curves for samples exposed to the thermal conditions I-III demonstrate both elastic and plastic domains while samples exposed in thermal condition IV demonstrate only elastic domain and fractured before the yield point (supporting figure S8 and S9 for TG1-1 and TG2-1, respectively). Consequently, Young's modulus (using equation 4), tensile strength, and the maximum elongation at break of the fabrics was determined and is plotted in Fig. 10 for thermal conditions I-IV. The Young's modulus of 41 ± 5 and 24 ± 2 MPa, the tensile strength of 30 ± 5 and 32 ± 5 MPa, and the elongation at break of 22 ± 4 and 13 ± 1 mm were obtained for the NH samples of TG1-1 and TG2-1, respectively. Under thermal condition II, no change in Young's modulus and the elongation at break was observed but a slight decrease in tensile strength (still within the margin of error) was observed. It means that the limited movement of polymer chains was unable to alter the mechanical properties of the fabrics.

A noticeable increase in Young's modulus, a decrease in the tensile strength and the elongation at break were observed (Fig. 10) for the samples exposed to the thermal condition III. This can be explained by the fibrillar to the lamellar transformations within the fibers which causes an increase in lamellar spacing and crystallinity. In general, the increase in the crystallinity (lamellar domains) which acts as rigid fillers and connectors between the polymer chains supports the increase in Young's modulus [41,42,46–48]. Therefore, fabrics treated under this thermal condition get relatively stiffer compared to NH samples due to the resistance of the materials to deform elastically under tensile load. Subsequently, decreasing behavior in tensile strength and elongation at break is obtained. Interestingly, the sample exposed in the thermal condition III, only increase in exposure time (at the flux of 20 kW/m^2 for 30 and 60s) leads to more change in structure and mechanical properties. Therefore, the thermal history, flux, and duration of heat exposure have to be known in order to access the further usage of fabrics.

For the samples exposed in the thermal condition IV, a decrease in tensile strength and elongation at the break was observed compared to the NH samples as shown in Fig. 10 (b) and (c). Young's modulus was considerably increased compared to the NH sample then start to decrease upon a further increase in the temperature of the samples exposed in the same thermal condition as shown in Fig. 10 (a) for both

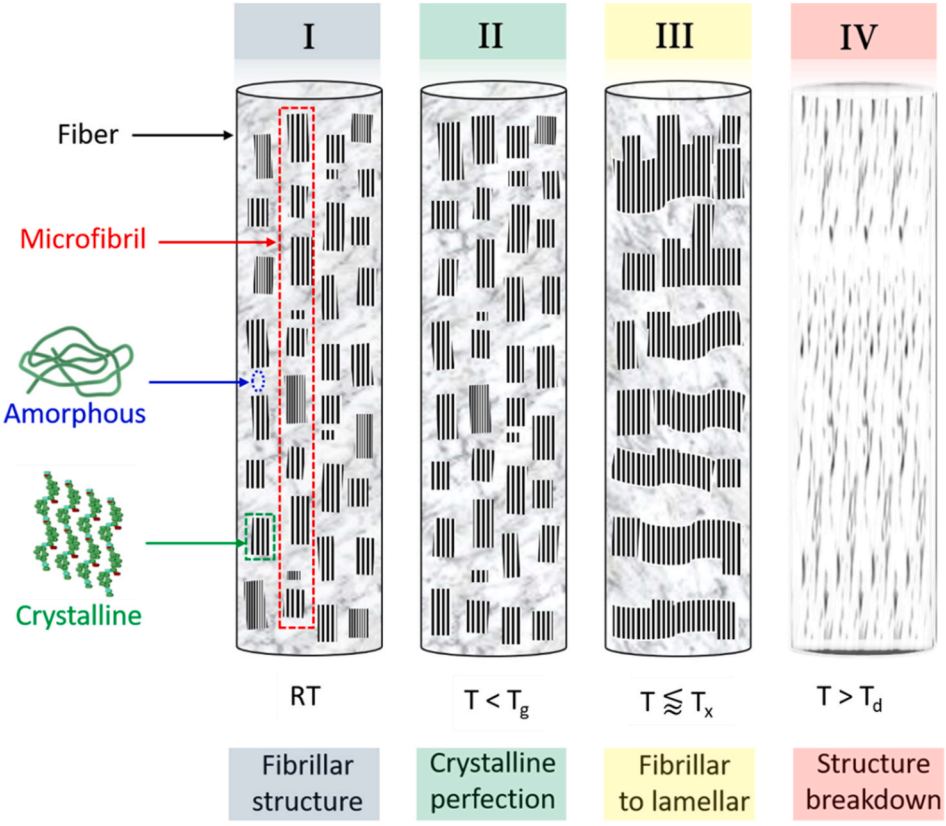

Fig. 9. Schematic of the structural changes within the outmost layer fibers exposed in the thermal conditions I – IV.

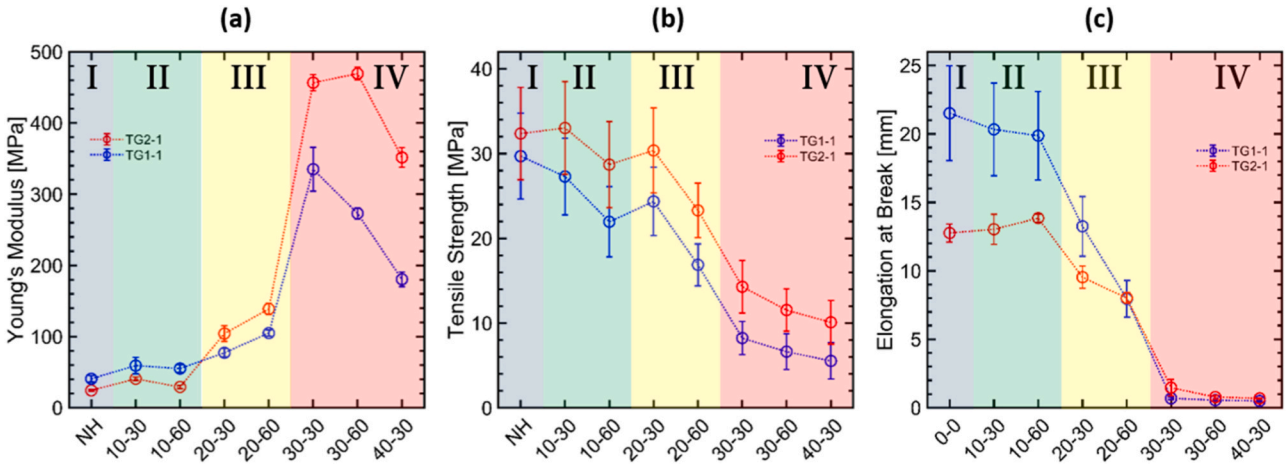

Fig. 10. (a) Young's modulus; (b) tensile strength; (c) maximum elongation at break of the samples exposed in the thermal conditions I-IV.

the fabrics. The reason for such a mechanical response of the fabrics can be explained by the thermal degradation of fibers as found in the SAXS, WAXD, and SEM characterization. As a consequence, the fabrics become brittle. Therefore, these samples do not exhibit a yield point and a plastic regime (supporting figure S8 and S9).

3.2. *Inner layers of the fabrics*

The inner layers of the thermal protective clothing are generally a moisture barrier and thermal liner to make up the assembly of the thermal protective fabric system. No change in the structure and mechanical behavior were observed in the inner layer (TG1-2) of the TG1 fabric system, which is discussed in the supporting information section S8. Furthermore, no major change in the structure and mechanical behavior were observed in the inner layers of the fabric system TG2 for I-IV thermal conditions except for TG2-2 and TG2-3Y for thermal condition IV. The structural changes were observed in TG2-2 and TG2-3Y for thermal condition IV that is in line with the change in their corresponding mechanical properties. However, for thermal condition IV, outermost layers of both fabrics were already degradaded. More details of the changes in the structural and mechanical properties of the TG2 fabric system is discussed in the supporting information section S9.The reason for inner layers remain mainly intact could be due to the fact that the temperature reached by the inner layers of both the fabric systems is not enough to generate the structural changes as these layers are protected by the outermost layer.

3.3. Assessment of the further usage of the fabric systems after heat exposures

The outermost layer of both fabric TG1-1 and TG2-1 showed similar structural and mechanical behavior when exposed to thermal condition I-IV. Both fabrics appear to be reusable even if exposed in thermal condition II. Combining SAXS, WAXD, and mechanical experiments, it was shown that fabrics exposed in the thermal condition III, when the temperature of the fabrics is in the proximity of the T_x for m-aramid, the mechanical integrity of the clothing during use could be jeopardized due to major structural transformations in the material which lead to an overall loss in mechanical strength. This thermal condition is of particular interest as no visible change in the fabric was observed under SEM. The results obtained for samples exposed in the thermal condition IV showed clearly that the fabric cannot be used further due to thermal degradation.

It was observed that the inner layer of the TG1 fabric system (i.e. TG1-2) is still intact for all four thermal conditions while inner layers of TG2 fabric system remains intact for thermal condition I-III but changes in structure and mechanical properties were observed for thermal condition IV. However, TG2-3G layer of TG2 fabric system remains intact for all the thermal conditions. The reason for intacting the properties of inner layers of the both fabrics could be mainly due to the protection of outermost layer which degraded in thermal condition IV. Therefore, the bottleneck for further usage of both fabric systems could be their outermost layers due to their compromised mechanical strength.

4. Conclusion

Two multilayer thermal protective fabric systems were exposed to I-IV thermal conditions to understand the structure-mechanical property relationship. Thermal analysis revealed the typical transitions of polymeric materials and allowed a quantification of the characteristic transitions to facilitate the correlation with the observed changes in structure by SEM, SAXS, and WAXD. We observed that the outermost layer of both fabrics was the most affected due to the highest level of heat exposures, which change them structurally in the thermal condition II & III and finally degraded in thermal condition IV. A slight increase in crystallinity but no change in the lamellar spacing was observed in the outermost layer fabric samples exposed under the thermal condition II compared to the NH samples. This was explained by the limited movement of the polymer chains within the fibers of the fabrics, which leads the crystalline perfection as the temperature of this thermal condition remained below the glass transition temperature of m-aramid fibers. Consequently, no change in mechanical properties at the fabric was observed. These results indicate that the fabric can be used again safely. Thermal condition III was of particular interest in this study because no change in the fabric was observed under SEM. A noticeable increase in the lamellar spacing and crystallinity was observed in the samples exposed in this thermal condition due to the fibrillar-to-lamellar transformation as the temperature in this thermal condition reaches in the proximity of 375 °C. As a consequence, significantly compromised mechanical properties were obtained compared NH sample. Therefore, even though no microscopic change in the fabric was observed under SEM, the further use of the fabric could be potentially dangerous to the end-user. In thermal condition IV, the SAXS correlation peak and main WAXD refection peaks of the m-aramid fibers were not observed which means that the molecular structure breakdown of the fibers have occurred. Thermal degradation of the fabric was also observed directly under SEM that led to the brittleness of the fabric. No changes in the inner layers of both fabrics in the thermal I-IV except TG2-2 and TG2-3Y layers which changes only in the thermal condition IV. However, in thermal condition IV, the outermost layers of both fabrics were already degraded. Therefore, the outermost layer could be the bottleneck for further usage of the fabric systems.

This study provides an in-depth understanding of the molecular interpretation of structural changes, which is in line with changes in the mechanical properties of thermal protective fabrics exposed to different heat conditions. Such knowledge supports improving the design and the fabrication processes with respect to the thermal performance of thermal protective fabrics. We show that changes in the internal structure of the fabrics can remain undetected by common analysis and require a multiscale analysis to successfully be put in evidence. By understanding and detecting these changes, one can develop a better appreciation of the requirements for thermal protective fabrics.

Author's contribution

RMR, AS, SA designed the study. AKM performed SEM, SAXS, and WAXD experiments and data analysis. SM, DEW, MS, MC contributed to radiant heat exposure and tensile measurement. JS and GF performed and analyzed the TGA and DSC measurements. AKM, AD, AN, AS, RMR contributed to the interpretation of the results. AKM wrote the manuscript from critical feedback and help from all the authors.

Declaration of competing interest

The authors declare that they have no known competing financial interests or personal relationships that could have appeared to influence the work reported in this paper.

Acknowledgment

The authors are grateful to the Swiss National Science Foundation (Project No. 173012) for financial support. The authors also thank Mr. Markus Hilber (Empa, Swiss Federal Laboratories for Materials Science and Technology, Advanced fibers, St. Gallen, Switzerland) for his support in mechanical measurement of the fabrics.

Appendix A. Supplementary data

Supplementary data to this article can be found online at https://doi.org/10.1016/j.polymer.2021.123634.

References

[1] S.A. Kahn, et al., Firefighter burn injuries: predictable patterns influenced by turnout gear, J. Burn Care Res. 33 (1) (2012) 152–156.
[2] R.M. Rossi, W. Bolli, R. Stampfli, Performance of firefighters' protective clothing after heat exposure, Int. J. Occup. Saf. Ergon. 14 (1) (2008) 55–60.
[3] C. Arrieta, et al., Thermal aging of a blend of high-performance fibers, J. Appl. Polym. Sci. 115 (5) (2010) 3031–3039.
[4] Q.Q. Feng, Zhu, J.F. Hu, Estimation of the radiant performance of flame-retardant fabrics considering thermal degradation effect. Journal of Engineered Fibers and Fabrics 14 (2019) 10.
[5] C. Arrieta, et al., X-ray diffraction, Raman, and differential thermal Analyses of the thermal Aging of a Kevlar (R)-PBI blend fabric, Polym. Compos. 32 (3) (2011) 362–367.
[6] G. Song, S. Mandal, R.M. Rossi, Thermal protective clothing for firefighters. Thermal Protective Clothing for Firefighters, Woodhead Publ Ltd, Cambridge, 2017, pp. 1–223.
[7] M. Fulton, M. Rezazadeh, D. Torvi, 5-Tests for Evaluating Textile Aging, in: P. Dolez, O. Vermeersch, V. Izquierdo (Eds.), Advanced Characterization and Testing of Textiles, Woodhead Publishing, 2018, pp. 93–125.
[8] P.I. Dolez, N.S. Tomer, Y. Malajati, A quantitative method to compare the effect of thermal aging on the mechanical performance of fire protective fabrics, J. Appl. Polym. Sci. 136 (6) (2019) 47045.
[9] M. Schmid, et al., Determination of critical heat transfer for the prediction of materials damages during a flame engulfment test, Fire Mater. 40 (8) (2016) 1036–1046.
[10] M. McQuerry, E. DenHartog, R. Barker, Evaluating turnout composite layering strategies for reducing thermal burden in structural firefighter protective clothing systems, Textil. Res. J. 87 (10) (2016) 1217–1225.
[11] M. Jassal, S. Ghosh, Aramid fibres - an overview, Indian J. Fibre Text. Res. 27 (3) (2002) 290–306.
[12] S. Ran, et al., Structural changes during deformation of Kevlar fibers via on-line synchrotron SAXS/WAXD techniques, Polymer 42 (4) (2001) 1601–1612.
[13] A.K. Maurya, et al., Structural insights into semicrystalline states of electrospun nanofibers: a multiscale analytical approach, Nanoscale 11 (15) (2019) 7176–7187.

[14] E.W. Fischer, Effect of annealing and temperature on the morphological structure of polymers, in: Pure and Applied Chemistry, 1972, p. 113.
[15] N.S. Murthy, et al., Drawing and annealing OF NYLON-6 fibers - studies OF crystal-growth, orientation OF amorphous and crystalline domains and their influence ON properties, Polymer 36 (20) (1995) 3863–3873.
[16] N.S. Murthy, H. Minor, R.A. Latif, Effect OF annealing ON the structure and morphology OF NYLON-6 fibers, J. Macromol. Sci. Phys. B26 (4) (1987) 427–446.
[17] G.S.Y. Yeh, et al., Annealing effects OF polymers and their underlying molecular mechanisms, Polymer 17 (4) (1976) 309–318.
[18] N.S. Murthy, D.T. Grubb, Deformation of lamellar structures: simultaneous small- and wide-angle X-ray scattering studies of polyamide-6, J. Polym. Sci. B Polym. Phys. 40 (8) (2002) 691–705.
[19] R. Rossi, Fire fighting and its influence on the body, Ergonomics 46 (10) (2003) 1017–1033.
[20] T. Sabir, *2-Fibers Used for High-Performance Apparel*, in *High-Performance Apparel*, in: J. McLoughlin, T. Sabir (Eds.), Woodhead Publishing, 2018, pp. 7–32.
[21] S. Bourbigot, X. Flambard, Heat resistance and flammability of high performance fibres: a review, Fire Mater. 26 (4–5) (2002) 155–168.
[22] J. Brown, B.C. Ennis, Thermal analysis of Nomex® and Kevlar® fibers, Textil. Res. J. 47 (1977) 62–66.
[23] S. Villar Rodil, A. Martinez Alonso, J.M.D. Tascón, Studies on pyrolysis of Nomex polyaramid fibers, J. Anal. Appl. Pyrol. (2001) 105–115, 58-59.
[24] T. Li, A.J. Senesi, B. Lee, Small angle X-ray scattering for nanoparticle research, Chem. Rev. 116 (18) (2016) 11128–11180.
[25] J. Li, et al., Application of the small-angle X-ray scattering technique for structural analysis studies: a review, J. Mol. Struct. 1165 (2018) 391–400.
[26] A.A. Coelho, TOPAS and TOPAS-Academic: an optimization program integrating computer algebra and crystallographic objects written in C plus, J. Appl. Crystallogr. 51 (2018) 210–218.
[27] H.M. Rietveld, A profile refinement method for nuclear and magnetic structures, J. Appl. Crystallogr. 2 (1969), 65-&.
[28] H.M. Rietveld, Line profiles OF neutron powder-diffraction peaks for structure refinement, Acta Crystallogr. 22 (1967), 151-&.
[29] H. Zhao, Y. Zhu, L. Sha, Study of the relationship between characteristics of aramid fibrids and mechanical property of aramid paper using DSC, E-Polymers 14 (2) (2014) 139–144.
[30] H.P. Zhang, et al., Effects of polar solvent on the structure and properties of M-aramid fibers, Adv. Mater. Res. 441 (2012) 169–173.
[31] Y.P. Khanna, E.M. Pearce, *Aromatic polyamides. V. Substituent effect on thermal properties.* Journal of applied polymer science 27 (6) (1982) 2053–2064.
[32] M.R. Roenbeck, et al., Structure-property relationships of aramid fibers via X-ray scattering and atomic force microscopy, J. Mater. Sci. 54 (8) (2019) 6668–6683.
[33] G. Porod, *Die Röntgenkleinwinkelstreuung von dichtgepackten kolloiden Systemen.* Kolloid-Zeitschrift 124 (2) (1951) 83–114.
[34] J. Petermann, M. Miles, H. Gleiter, Growth OF polymer crystals during annealing, J. Macromol. Sci. Phys. 12 (3) (1976) 393–404.
[35] E.W. Fischer, *Small angle X-RAY scattering studies OF phase transitions IN polymeric and OLIGOMERIC systems.* Pure appl. Chem 31 (1972) 113.
[36] J.M. Schultz, J. Petermann, Transmission electron microscope observations of fibrillar-to-lamellar transformations in melt-drawn polymers — I, Isotactic polypropylene. Colloid and Polymer Science 262 (4) (1984) 294–300.
[37] J. Loboda-Čačković, H. Čačković, R. Hosemann, The analysis of four point diagrams of branched, cold stretched polyethylene, J. Polym. Sci., Polym. Symp. 42 (2) (1973) 577–589.
[38] H. Kakida, Y. Chatani, H. Tadokoro, Crystal structure of poly(m-phenylene isophthalamide), J. Polym. Sci. Polym. Phys. Ed 14 (3) (1976) 427–435.
[39] M.G. Northolt, X-RAY-DIFFRACTION study OF poly(P-phenylene terephthalamide) fibers, Eur. Polym. J. 10 (9) (1974) 799–804.
[40] S. Hayashi, *GROWTH HABITS OF POLYMER SINGLE-CRYSTALS.* Polymer journal 7 (4) (1975) 415–422.
[41] W.R. Krigbaum, R.J. Roe, K.J. Smith, A theoretical treatment OF the modulus OF semi-crystalline polymers, Polymer 5 (10) (1964) 533–542.
[42] J.W.S. Hearle, The structural mechanics of fibers, J. Polym. Sci. Part C: Polymer Symposia 20 (1) (1967) 215–251.
[43] Z. Zupin, K. Dimitrovski, Mechanical properties of fabrics made from cotton and biodegradable yarns bamboo, SPF, PLA in weft, in woven fabric engineering, 2010.
[44] J. Hu, 4-The Tensile Properties of Woven Fabrics, in: J. Hu (Ed.), Structure and Mechanics of Woven Fabrics, Woodhead Publishing, 2004, pp. 91–122.
[45] J. Hu, B. Xin, 3-Structure and Mechanics of Woven Fabrics, in: P. Schwartz (Ed.), Structure and Mechanics of Textile Fibre Assemblies, Woodhead Publishing, 2008, pp. 48–83.
[46] L.E. Nielsen, F.D. Stockton, Theory of the modulus of crystalline polymers, J. Polym. Sci. - Part A Gen. Pap. 1 (6) (1963) 1995–2002.
[47] S. Humbert, et al., A re-examination of the elastic modulus dependence on crystallinity in semi-crystalline polymers, Polymer 52 (21) (2011) 4899–4909.
[48] A. Morel, et al., Correlating diameter, mechanical and structural properties of poly (L-lactide) fibres from needleless electrospinning, Acta Biomater. 81 (2018) 169–183.